Japanese Journal of Radiology (2019) 37:117–134
https://doi.org/10.1007/s11604-018-0777-5

INVITED REVIEW

CT-based mediastinal compartment classifications and differential diagnosis of mediastinal tumors

Takahiko Nakazono[1] · Ken Yamaguchi[1] · Ryoko Egashira[1] · Yukari Takase[2] · Junichi Nojiri[1] · Masanobu Mizuguchi[1] · Hiroyuki Irie[1]

Received: 16 July 2018 / Accepted: 10 September 2018 / Published online: 20 September 2018

Abstract
Division of the mediastinum into compartments is used to help narrow down the differential diagnosis of mediastinal tumors, assess tumor growth, and plan biopsies and surgical procedures. There are several traditional mediastinal compartment classification systems based upon anatomical landmarks and lateral chest radiograph. Recently, the Japanese Association of Research of the Thymus (JART) and the International Thymic Malignancy Interest Group (ITMIG) proposed new mediastinal compartment classification systems based on transverse CT images. These CT-based classification systems are useful for more consistent and exact diagnosis of mediastinal tumors. In this article, we review these CT-based mediastinal compartment classifications in relation to the differential diagnosis of mediastinal tumors.

Keywords Mediastinum · Compartment · Computed tomography · Magnetic resonance imaging

Introduction

The mediastinum is anatomically bound on the lateral side by the parietal pleural reflections along the medial aspects of both lungs, superiorly by the thoracic inlet, inferiorly by the diaphragm, anteriorly by the sternum, and posteriorly by the thoracic vertebral bodies. Various tumors and tumor-like lesions occur in the mediastinum. It is thus clinically important to have a standardized system that can classify the mediastinum into several compartments in order to assess the origin and extension of mediastinal lesions. There are several traditional mediastinal classifications based on anatomy and chest radiographs [1–6]. Felson proposed 3-mediastinal compartment classification method based on the lateral chest radiographs [2], resulting in a widely used classification that is both simple and diagnostically useful. However, differences in terminology and methods have resulted in confusion among physicians. In addition, the traditional models are based on lateral chest radiographs, and thus some mediastinal lesions cannot be reliably localized to a specific compartment, since considerable overlap exists among the radiographically imaged compartments. Because mediastinal lesions are optimally evaluated with cross-sectional imaging techniques, computed tomography (CT) is currently the main practical clinical examination for assessing the existence, origin and extension of mediastinal tumors. The Japanese Association of Research of the Thymus (JART) proposed a CT-based 4-compartment mediastinal classification system [7]. The International Thymic Malignancy Interest Group (ITMIG) subsequently modified the JART classification system to produce a CT-based 3-compartment mediastinal classification system [8]. In this article, we review the new CT-based mediastinal compartment classifications and discuss their use in the differential diagnosis of mediastinal tumors.

✉ Takahiko Nakazono
nakazot@cc.saga-u.ac.jp

[1] Department of Radiology, Faculty of Medicine, Saga University, Nabeshima 5-1-1, Saga City, Saga 849-8501, Japan

[2] Departments of Pathology & Microbiology, Faculty of Medicine, Saga University, Nabeshima 5-1-1, Saga City, Saga 849-8501, Japan

CT-based mediastinum compartment classifications

Sone et al. [9] evaluated CT images from 15 patients after pneumomediastinography and described two potential mediastinal spaces. The anterior (precardiovascular) zone

is anterior to the superior vena cava, brachiocephalic artery, aorta, left common carotid artery, left subclavian artery, and heart. The anterior zone is described as extending laterally to surround the heart. The central (retrocardiovascular) zone is an area around the trachea and esophagus and anterior to the vertebrae [9].

Fujimoto et al. [7] from JART proposed a new CT-based 4-compartment mediastinal classification system that included the superior portion of the mediastinum, anterior mediastinum (prevascular zone), middle mediastinum (peritracheoesophageal zone), and posterior mediastinum (paravertebral zone) (Fig. 1). The boundaries of each compartment are shown in Table 1 [7]. The inferior boundary of the superior portion of the mediastinum is a horizontal plane at the intersection of the caudal margin of the brachiocephalic vein with the trachea. Classifying the superior portion of the mediastinum has the advantage of making it easy to differentiate an intrathoracic goiter or neurogenic tumor of the thoracic inlet from other mediastinal tumors [7]. The lateral boundaries of the anterior mediastinum are the parietal (mediastinal) pleural reflections (including the lateral rims of the bilateral internal thoracic arteries and veins, and the superior and inferior pulmonary veins). The posterior boundary of the anterior mediastinum is formed by the pericardium (including a horizontal line at the posterior rim of the heart), anterior rims of the left brachiocephalic vein, superior vena cava, superior and inferior pulmonary veins, ascending aorta, and lateral rim of the aortic arch. The anterior boundary of the middle mediastinum consists of the posterior rim of the left brachiocephalic vein, superior vena cava, ascending aorta, bilateral main pulmonary arteries, and the heart. The posterior boundary of the middle mediastinum consists of the anterior rim of the descending aorta and a vertical line connecting a point on each thoracic vertebral body at 1 cm behind its anterior margin [middle-posterior boundary line (M-PBL), red dotted lines in Fig. 1]. The middle mediastinum includes mainly the trachea, bilateral main bronchi and esophagus. The posterolateral boundaries of the superior portion of the mediastinum and the posterior mediastinum are vertical lines against the posterior rim of the chest wall at the lateral rim of the thoracic vertebral transverse process (yellow solid lines in Fig. 1) [7]. Fujimoto et al. [7] evaluated the JART CT-based classification method by using it to assess 445 mediastinal mass lesions and reported that the classification was

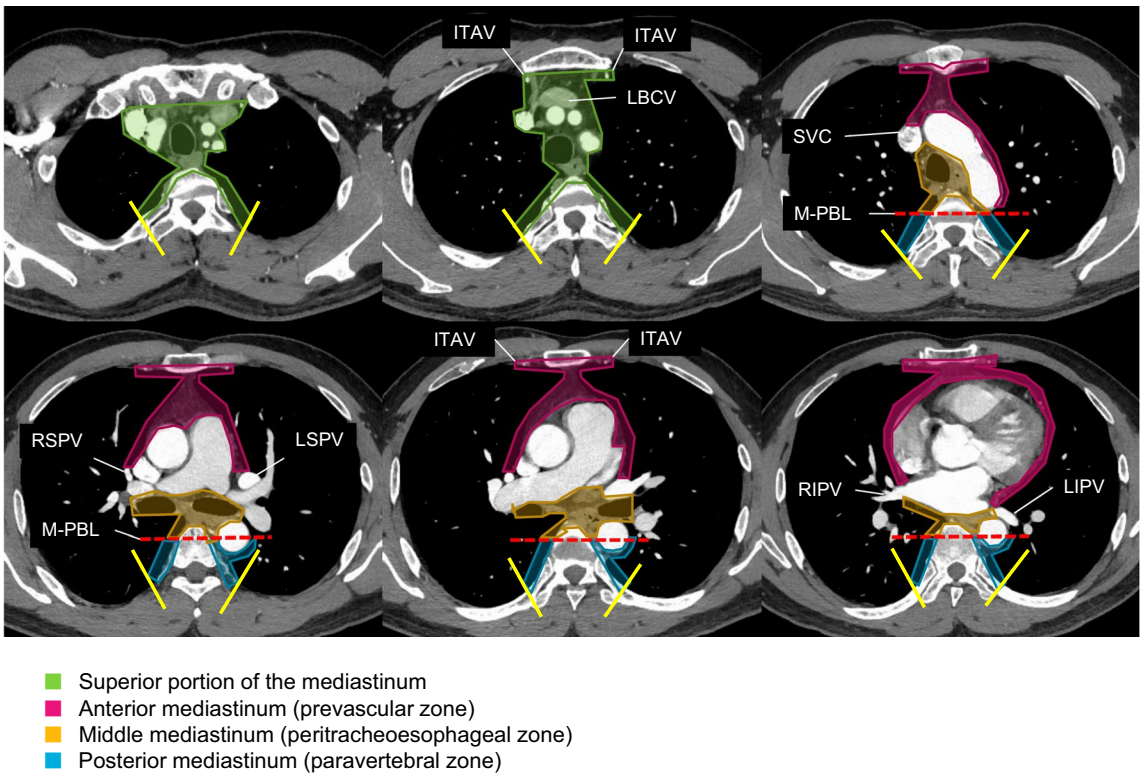

Fig. 1 Axial contrast-enhanced CT images representing the JART CT-based mediastinal compartment classification [7]. JART: The Japanese Association for Research on the Thymus; LBCV, left brachiocephalic vein; ITAV, internal thoracic arteries and veins; SVC, superior vena cava; RSPV, right superior pulmonary vein; LSPV, left superior pulmonary vein; RIPV, right inferior pulmonary vein; LIPV, left inferior pulmonary vein; M-PBL, middle-posterior boundary line (a vertical line connecting a point on each thoracic vertebral body at 1 cm behind its anterior margin)

Table 1 Anatomical boundaries of the JART CT-based mediastinal compartment classification [7]

Compartments	Boundaries
Superior portion of the mediastinum	Superior: thoracic inlet Inferior: horizontal plane at the intersection of the caudal margin of the LBCV with the trachea Posterior: anterior rim of the thoracic vertebral body Posterior-lateral: vertical line against the posterior rim of the chest wall at the lateral rim of the thoracic vertebral process
Anterior mediastinum (prevascular zone)	Superior: inferior boundary of the superior portion of the mediastinum Inferior: diaphragm Lateral: parietal (mediastinal) pleural reflections, ITAV, RSPV, LSPV, RIPV, and LIPV Posterior: pericardium, anterior rims of the LBCV, SVC, RSPV, LSPV, RIPV, LIPV, ascending aorta, and lateral rim of the aortic arch
Middle mediastinum (peritracheoesophageal zone)	Superior: inferior boundary of the superior portion of the mediastinum Inferior: diaphragm Anterior: posterior rim of the LBCV, SVC, ascending aorta, bilateral main pulmonary arteries, and heart Posterior: anterior rim of the descending aorta and M-PBL
Posterior mediastinum (paravertebral zone)	Superior: inferior boundary of the superior portion of the mediastinum Inferior: diaphragm Anterior: M-PBL Posterior-lateral: vertical line against the posterior rim of the chest wall at the lateral rim of the thoracic vertebral process

JART, The Japanese Association for Research on the Thymus, LBCV, left brachiocephalic vein; ITAVs, internal thoracic arteries and veins; SVC, superior vena cava; RSPV, right superior pulmonary vein; LSPV, left superior pulmonary vein; RIPV, right inferior pulmonary vein; LIPV, left inferior pulmonary vein; M-PBL, middle-posterior boundary line (a vertical line connecting a point on each thoracic vertebral body at 1 cm behind its anterior margin)

sufficiently user-friendly and potentially useful for the differential diagnosis of mediastinal lesions.

ITMIG modified and simplified the JART classification to produce a CT-based 3-compartment classification that has the advantages of similarity to the published anatomic, clinical, and radiologic 3-compartment models currently used, a less complicated design, and the use of true anatomic planes to establish compartmental boundaries [8]. The ITMIG CT-based classification includes the prevascular (anterior), visceral (middle), and paravertebral (posterior) compartments (Fig. 2) [8]. The boundaries of each compartment are shown in Table 2 [8]. The posterior boundary of the prevascular compartment is the anterior aspect of the pericardium as it wraps around in a curvilinear fashion. Based on these landmarks, the major contents of the prevascular compartment include the thymus, fat, lymph nodes, and left brachiocephalic vein. The anterior boundary of the visceral compartment is the anterior aspect of the pericardium (which envelops the distal aspect of the superior vena cava, the proximal aspect of the ascending aorta and the lateral rim of the aortic arch, and the intrapericardial pulmonary arteries), and the posterior boundary is a vertical line connecting a point on the thoracic vertebral bodies 1 cm posterior to the anterior margin of the spine [visceral–paravertebral compartment boundary line (V-PBL), red dotted lines in Fig. 2]. The major contents of the visceral compartment include two main components: (1) a vascular component (i.e., the heart, superior vena cava, ascending thoracic aorta, aortic arch, and descending thoracic aorta, intrapericardial pulmonary arteries, and the thoracic duct) and (2) the trachea, carina, esophagus, and lymph nodes [8].

In the JART classification, the heart and great vessels are not included in the mediastinum compartments [7]. In contrast, all structures within the pericardium are included in the visceral compartment in the ITMIG classification [8]. Because the superior portion of the mediastinum in the JART classification is a narrow space, some lesions in the location may be difficult to classify according to the ITMIG classification.

Differential diagnosis of mediastinal tumors according to the CT-based mediastinal compartment classifications

Table 3 shows the differential diagnosis of solid and cystic mediastinal tumors according to the JART and ITMIG CT-based mediastinal compartment classifications. Tumor location and imaging features are key to the differential diagnosis of mediastinal tumors.

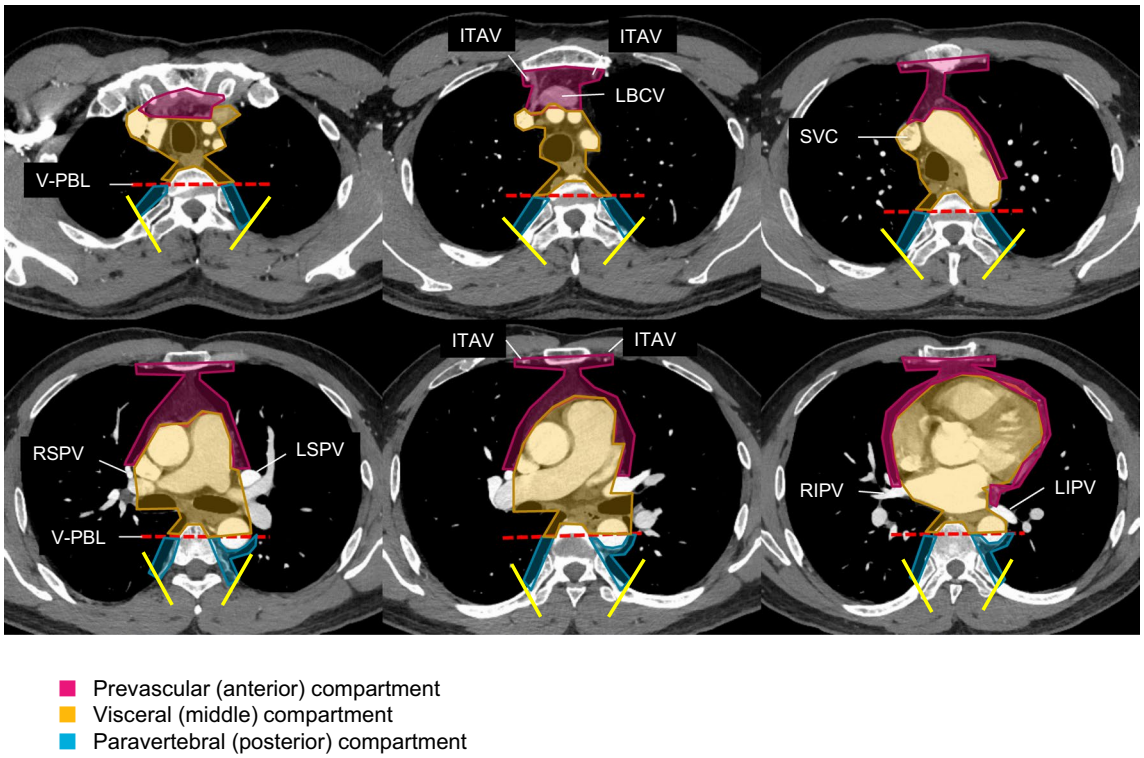

Fig. 2 Axial contrast-enhanced CT images representing the ITMIG CT-based mediastinal compartment classification [8]. ITMIG: The International Thymic Malignancy Interest Group; LBCV, left brachiocephalic vein; ITAV, internal thoracic arteries and veins; SVC, superior vena cava; RSPV, right superior pulmonary vein; LSPV, left superior pulmonary vein; RIPV, right inferior pulmonary vein; LIPV, left inferior pulmonary vein; V-PBL, visceral-paravertebral compartment boundary line (a vertical line connecting a point on each thoracic vertebral body at 1 cm behind its anterior margin)

Table 2 Anatomical boundaries of the ITMIG CT-based mediastinal compartment classification [8]

Compartments	Boundaries
Prevascular (Anterior)	Superior: thoracic inlet Inferior: diaphragm Lateral: parietal (mediastinal) pleural reflections, ITAV, RSPV, LSPV, RIPV, and LIPV Posterior: pericardium, SVC, RSPV, LSPV, RIPV, LIPV, ascending aorta, and lateral rim of the aortic arch
Visceral (Middle)	Superior: thoracic inlet Inferior: diaphragm Anterior: posterior boundaries of the prevascular compartment Posterior boundary: V-PBL
Paravertebral (Posterior)	Superior: thoracic inlet Inferior: diaphragm Anterior: posterior boundary of the visceral compartment Posterior-lateral: vertical line against the posterior margin of the chest wall at the lateral margin of the transverse process of the thoracic spine

ITMIG, The International Thymic Malignancy Interest Group; LBCV, left brachiocephalic vein; ITAV, internal thoracic arteries and veins; SVC, superior vena cava; RSPV, right superior pulmonary vein; LSPV, left superior pulmonary vein; RIPV, right inferior pulmonary vein; LIPV, left inferior pulmonary vein; V-PBL, visceral-paravertebral compartment boundary line (a vertical line connecting a point on each thoracic vertebral body at 1 cm behind its anterior margin)

Superior portion of the mediastinum (JART)

Thyroid lesions and neurogenic tumors are common in this compartment. Ectopic thymus results from defective pathways of the embryologic descent of the thymus, and thymic lesions can occur anywhere along the path of the thymopharyngeal duct in the neck and in this compartment.

Table 3 Differential diagnosis of mediastinal tumors according to the CT-based mediastinal compartment classifications

JART	Superior portion of the mediastinum	Anterior mediastinum	Middle mediastinum	Posterior mediastinum
ITMIG		Prevascular compartment	Visceral compartment	Paravertebral compartment
Solid	Intrathoracic goiter Parathyroid tumors Peripheral nerve tumors Sympathetic nerve tumors Paraganglioma Thymic tumors Lymph node lesions	Thymic tumors Malignant lymphoma Germ cell tumors Intrathoracic goiter Peripheral nerve tumors Paraganglioma Lymph node lesions	Lymph node lesions Intrathoracic goiter Peripheral nerve tumors Paraganglioma	Peripheral nerve tumors Sympathetic nerve tumors Paraganglioma Lymph node lesions Extramedullary hematopoiesis Myelolipoma
Cystic	Thyroid cyst Parathyroid cyst Neurogenic tumors with cystic change Thymic cyst Bronchogenic cyst Lateral menigocele Neurenteric cyst Thoracic duct cyst Cystic lymphangioma	Thymic cyst Pericardial cyst Cystic teratoma Cystic lymphangioma	Bronchogenic cyst Esophageal cyst Pericardial cyst Thoracic duct cyst Pancreatic pseudocyst	Neurogenic tumors with cystic change Lateral menigocele Neurenteric cyst Thoracic duct cyst Pancreatic pseudocyst

JART, The Japanese Association of Research of the Thymus; ITMIG, The International Thymic Malignancy Interest Group

Intrathoracic goiter

The majority of intrathoracic goiters are substernal extensions of cervical goiters. They commonly occur in the superior portion of the mediastinum (JART) or prevascular compartment (ITMIG) and may extend to the other compartments. Rare cases (less than 1%) show no evident connection to the cervical thyroid gland and are thought to arise from an ectopic thyroid gland in the mediastinum (Fig. 3) [10]. Adenomatous goiter is the most common histologically,

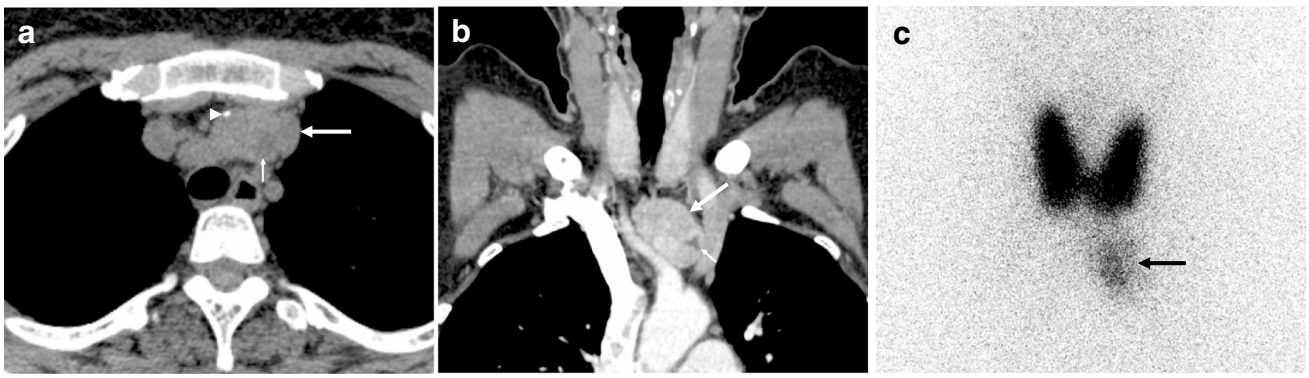

Fig. 3 Intrathoracic goiter in a 49-year-old woman. An axial plain CT image shows a well-circumscribed nodule (large arrow) with a small calcification (arrowhead) and cystic change (small arrow) in the superior portion of the mediastinum (JART). **a** A coronal contrast-enhanced CT image shows heterogeneous enhancement of the nodule (large arrow) with cystic change (small arrow). There is no connection between the nodule (large arrow) and the thyroid gland. **b** A ^{123}I-scintigraphy image shows high accumulation of the lesion (arrow)

and carcinomas are rare (2–3% of cases) [10]. Adenomatous goiters usually show diffuse enlargement of the thyroid gland and multiple nodules. Calcification (Fig. 3a), cystic change (Fig. 3a, b), and hemorrhage are common in intrathoracic goiter. Intense and heterogeneous enhancement is seen on contrast-enhanced CT (Fig. 3b) and MRI. ^{123}I-scintigraphy is useful to detect thyroid tissues (Fig. 3c) [10].

Parathyroid lesions

Because of the likely common origin of the thymus and the inferior parathyroid glands from the third brachial pouch, 22% of parathyroid adenomas develop in the mediastinum in patients with hyperparathyroidism [11]. Mediastinal parathyroid adenomas are common in the superior portion of the mediastinum and the anterior mediastinum. Parathyroid adenomas are encapsulated, round, and usually small. The tumors show early and marked enhancement on contrast-enhanced CT and MRI. Parathyroid cysts and carcinomas rarely occur in the mediastinum.

Anterior mediastinum (JART), prevascular compartment (ITMIG)

Thymic epithelial tumors are the most common tumors in this compartment, and primary mediastinal malignant lymphomas and germ cell tumors usually occur here.

Thymic epithelial tumors

Thymomas occur at almost all ages, with a peak incidence at 55–65 years, and are associated with various autoimmune diseases such as myasthenia gravis, pure red cell anemia, Good's syndrome, Hashimoto's thyroiditis, lichen planus, Graves' disease, and inflammatory myopathy [12]. The World Health Organization (WHO) has histologically classified thymomas into types A, AB, B1, B2 and B3 [12]. Types A, AB, and B1 are reported to be low-risk while types B2 and B3 are high-risk. High-risk thymomas frequently show extracapsular invasion, and their prognosis is worse than that of low-risk thymomas [12]. Various histological subtypes of thymic carcinoma are included in the WHO classification, with the most common being squamous cell carcinoma [12]. Thymic carcinomas usually present at around 50 years of age.

Low-risk thymomas are likely to show a smooth contour on CT and MRI [13, 14] and a low-signal-intensity complete capsule in the periphery of the mass on T2-weighted images (Fig. 4a) [13]. Low-signal-intensity septa on T2-weighted images are common in thymomas (Fig. 4a) [13]. The peripheral capsule and septa within thymomas typically show gradual enhancement on dynamic contrast-enhanced MRI (Fig. 4b). High-risk thymomas and thymic carcinomas are likely to show an irregular contour [13, 14]. Calcification is frequent in types B1, B2, and B3 thymomas [14]. Cystic change (Fig. 4a) is common in thymomas. Pleural dissemination is frequent in high-risk thymomas. Thymic

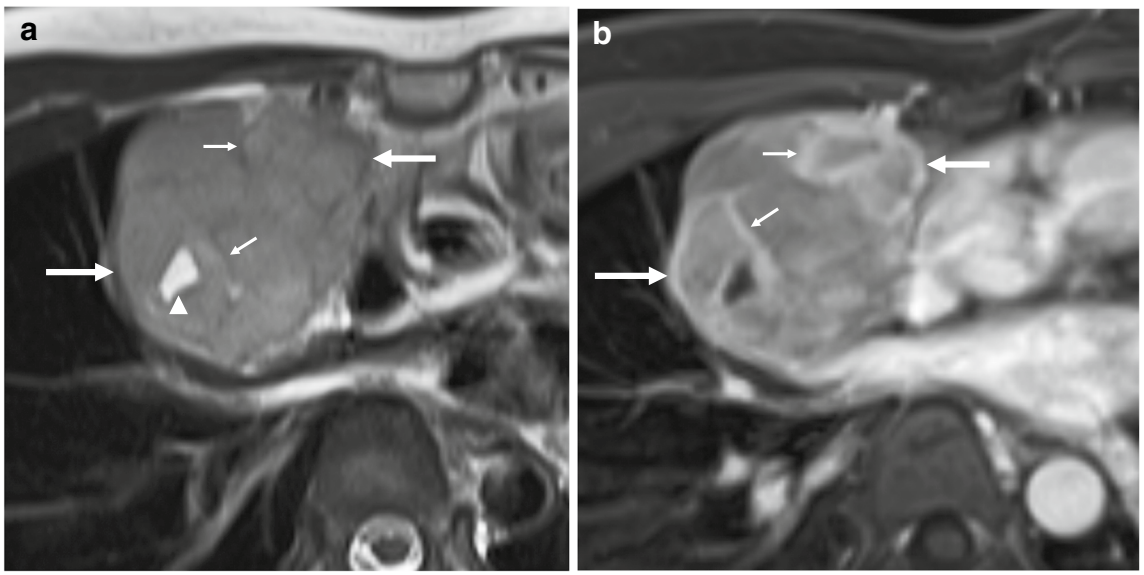

Fig. 4 Low-risk thymoma (type AB) in a 42-year-old woman. **a** An axial T2-weighted image shows a lobulated mass in the anterior mediastinum. Cystic change (arrowhead) is seen in the mass. The low-signal-intensity peripheral rim (large arrows) reflects the fibrous capsule of the tumor. Low-signal-intensity lines (small arrows) within the mass reflect fibrous septa. **b** An axial dynamic contrast-enhanced MR image (180 s after injection of contrast material) shows heterogeneous enhancement of the mass. Peripheral rim enhancement (large arrows) reflects the fibrous capsule of the tumor. Linear enhancement (small arrows) within the mass reflects fibrous septa in the tumor

carcinomas are likely to be heterogeneous due to tumor necrosis [13]. Lymph node and hematogenous metastases are common in thymic carcinomas and rare in thymomas.

Thymic neuroendocrine carcinomas are classified into typical carcinoid, atypical carcinoid, large cell neuroendocrine carcinoma (LCNEC), and small cell carcinoma in the WHO classification [12]. The majority of thymic neuroendocrine carcinomas are atypical carcinoids, which usually present at 40–50 years of age [12]. Differential diagnosis among thymic neuroendocrine carcinomas, thymomas, and thymic carcinomas is difficult. Thymic carcinoids are reported to show moderate to marked enhancement on contrast-enhanced CT (Fig. 5) and MRI [15, 16]. Vessels on contrast-enhanced CT (Fig. 5) and flow voids on MRI may be seen, reflecting tumor hypervascularity [15]. Lymph node and hematogenous metastases are common, and prognosis is poor in LCNECs and small cell carcinomas [12].

Thymic hyperplasia

Thymic hyperplasia is divided histologically into true hyperplasia and lymphoid hyperplasia. True thymic hyperplasia is defined as an increase in the size of the thymus with normal gross and histological appearance and commonly occurs as a rebound phenomenon secondary to atrophy caused by chemotherapy for malignancy or corticosteroid therapy, etc. [17]. Thymic lymphoid hyperplasia is pathologically diagnosed by the presence of hyperplastic lymphoid germinal centers in the medulla of the thymus, in association with a lymphocytic and plasma cell infiltrate. Thymic lymphoid hyperplasia is seen in more than 50% of patients with myasthenia gravis [17]. Thymic hyperplasia appears on CT and MRI as a round or box-shaped mass in children and a flat triangular mass in adults in the anterior mediastinum [17]. Differential diagnosis between rebound thymic hyperplasia and recurrence is very important in patients after chemotherapy for malignancies. Chemical shift MR imaging can detect tiny fat tissues in thymic hyperplasia and is therefore useful for differentiation from thymic epithelial tumors [18].

Fig. 5 Thymic atypical carcinoid in a 58-year-old man. An axial contrast-enhanced CT (arterial phase) shows a well-circumscribed mass (arrow) in the anterior mediastinum. The image shows heterogeneous enhancement of the mass (arrow) and vessels (arrowheads) in the mass and the periphery reflecting the hypervascularity of the tumor

Thymolipoma

Thymolipoma is a rare benign tumor that contains thymic and fat tissues. The average age of patients is 22–26 years and most patients are asymptomatic [19]. Thymolipomas typically show a large soft mass comprised of intermingling soft tissue and fat tissues in the anterior mediastinum [19].

Malignant lymphomas

Major histologic subtypes of primary mediastinal malignant lymphomas are primary mediastinal large B-cell lymphoma (PMBCL), nodular sclerosis Hodgkin lymphoma, and T-cell lymphoblastic lymphoma (T-LBL) [12, 20]. PMBCLs occur in younger adults with a peak incidence at 20–30 years. Nodular sclerosis Hodgkin lymphomas are common in young females. T-LBLs occur in children and young adults with a male predilection [12, 20]. Soluble interleukin-2 receptor (sIL-2R) is helpful for diagnosis of malignant lymphoma. PMBCLs show a large heterogeneous mass in the anterior mediastinum. Necrosis, cystic change and hemorrhage in the mass, and lymph node enlargement are frequent. Pleural and pericardial effusion are seen in about one-third of cases [17]. Nodular sclerosis Hodgkin lymphomas typically show a relatively homogeneous mass with limited necrosis and cystic change. Lymph node enlargement may be seen in regions adjacent to the primary lesion [17]. T-LBLs show a large heterogenous mass with necrosis (Fig. 6). Pleural and pericardial effusion (Fig. 6) and lymph node enlargements are common [20, 21]. T-LBLs typically show rapid enlargement of the mass, and patients complain of chest pain and dyspnea (Fig. 6) [17, 20]. Penetration of vessels may be seen in malignant lymphomas, since calcification is very rare prior to chemotherapy. Thymic extranodal marginal zone lymphoma of mucosa-associated lymphoid tissue (MALT lymphoma) is rare. Thymic MALT lymphoma is strongly associated with autoimmune diseases, especially Sjögren's syndrome [12]. Most patients with thymic MALT lymphoma are in their sixth or seventh decade and approximately 80% of reported cases have occurred in Asian patients [12].

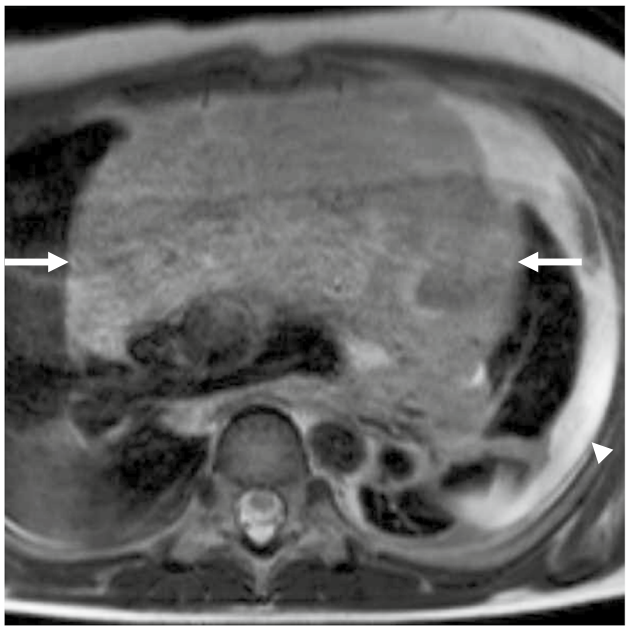

Fig. 6 T-cell lymphoblastic lymphoma in a 13-year-old boy who had chest pain and dyspnea. An axial T2-weighted image shows a large heterogeneous mass (arrows) in the anterior mediastinum. The mediastinal structures are displaced by the large mass. Left pleural effusion (arrowhead) is also seen

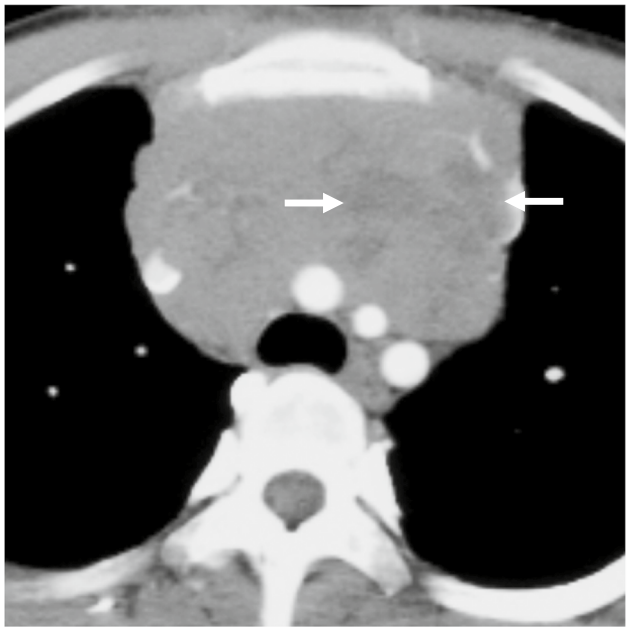

Fig. 7 Seminoma in a 38-year-old man. An axial contrast-enhanced CT shows a lobulated mass with relatively homogeneous enhancement in the anterior mediastinum. Small low-attenuation areas (arrows) within the mass reflect tumor necrosis

Thymic MALT lymphoma is associated with an excellent outcome. Thymic MALT lymphomas are reported to show a mass with cystic and solid components, a multilocular cyst, or a solid mass in the anterior mediastinum [22]. Differential diagnosis between thymic MALT lymphoma and multilocular thymic cyst is difficult in patients with Sjögren's syndrome.

Germ cell tumors

Generally, germ cell tumors consist of three categories: (1) teratomas (mature teratoma, immature teratoma, and teratoma with malignant transformation); (2) seminomas; and (3) nonseminomatous malignant germ cell tumors (embryonal carcinoma, yolk sac tumor, choriocarcinoma, and mixed germ cell tumor) [12, 17]. More than 80% of germ cell tumors are benign, with a large majority being mature teratomas [12, 17]. Mature teratomas occur with equal frequency in men and women, while malignant germ cell tumors have a predominant distribution in males during the second to fourth decades [12, 17]. Malignant germ cell tumors occasionally secrete tumor markers such as alpha-fetoprotein and human chorionic gonadotropin. Prognosis is worse in nonseminomatous germ cell tumors than in pure seminomas. The vast majority of mediastinal germ cell tumors arise within the anterior mediastinum; only 3% arise in the posterior mediastinum [12, 17].

On CT, mature teratomas commonly appear as thick-walled unilocular or multilocular cystic lesions containing fluid, soft tissue, and fat attenuation [23]. Calcifications are also present, and a tooth or piece of bone is seen on rare occasion. A fat-fluid level within the mass is characteristic for teratomas in general, but rare in mediastinal cases. Chemical shift MRI is useful to detect tiny amounts of fat tissue within the lesions. Nearly 30% of mature teratomas have been reported to rupture into adjacent structures [24]. Seminomas typically appear as relatively homogeneous masses on CT (Fig. 7) and MRI. Areas of degeneration due to hemorrhage and coagulation necrosis may be present but are usually limited (Fig. 7). Nonseminomatous germ cell tumors typically appear more heterogeneous, reflecting marked necrosis and hemorrhage in the tumor (Fig. 8), and lymph node and hematogenous metastases are common (Fig. 8) [25].

Thymic cysts

Congenital thymic cysts are derived from a remnant of the thymopharyngeal duct and are usually unilocular and generally small [26]. Acquired thymic cysts, occasionally referred to as multilocular thymic cysts, are associated with Sjögren's syndrome, human immunodeficiency virus infection, and various neoplasms including thymic carcinomas [26]. Multilocular thymic cysts contain serous, viscous, and/or hemorrhagic (motor-oil-like) fluid.

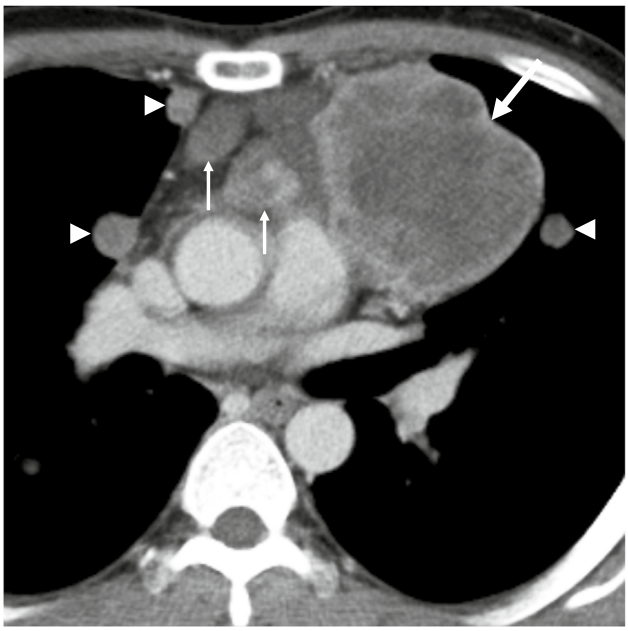

Fig. 8 Nonseminomatous germ cell tumor (embryonal carcinoma) in a 32-year-old man. An axial contrast-enhanced CT shows a lobulated mass (large arrow) with heterogeneous enhancement in the anterior mediastinum. Large central low-attenuation areas within the mass reflect tumor necrosis. Mediastinal lymph node metastases (small arrows) and lung metastases (arrowheads) are also seen

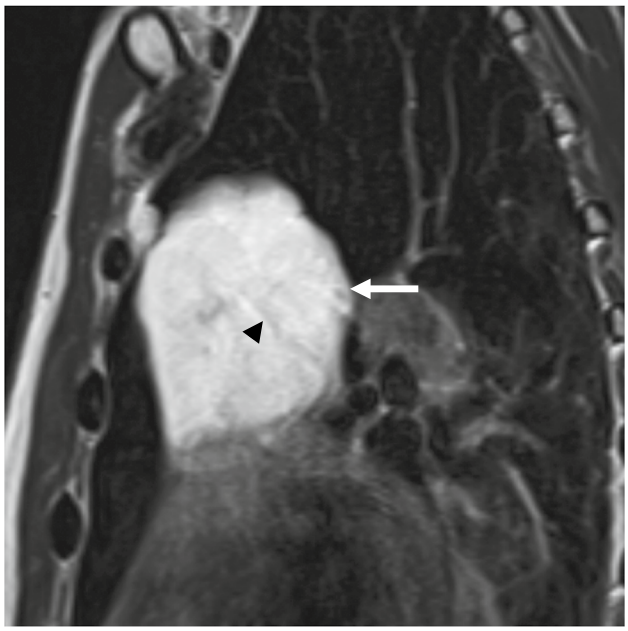

Fig. 9 Cystic lymphangioma in a 56-year-old man. A sagittal T2-weighted image shows a multilocular cystic mass (arrow) with thin septa (arrowhead) in the anterior mediastinum

Pericardial cyst

Pericardial (mesothelial) cysts result from aberrations in the formation of coelomic cavities. The cyst walls are composed of connective tissue and a single layer of mesothelial cells [26]. The majority of pericardial cysts are located in the cardiophrenic angles, more frequently on the right side. Pericardial diverticulum has been found as high as the pericardial recesses at the level of the proximal aorta and pulmonary arteries [26]. A pericardial cyst typically appears as a thin-walled unilocular cyst containing serous fluid.

Lymphangioma

Lymphangioma is a benign tumor of neoplastic or hamartomatous nature, composed of proliferating lymphatic vessels containing chylous material and varying in size, grossly appearing as cystic or spongy [27]. Lymphangiomas are rare in the mediastinum (1% of all lymphangiomas), and reported cases typically occupy the superior portion of the mediastinum and the anterior mediastinum [27]. They are classified histologically as simple (capillary), cavernous, or cystic (hygroma), depending on the size of the lymphatic channels they contain. Cystic lymphangiomas are the most common and may be either unilocular or multilocular. Thin septa within the mass can sometimes be seen (Fig. 9) [27].

Middle mediastinum (JART), visceral compartment (ITMIG)

The most common solid lesions in this compartment are lymph node lesions including metastases, malignant lymphoma, and granulomatous diseases such as sarcoidosis, sarcoid reaction, tuberculosis, and silicosis. Foregut cysts including bronchogenic cysts and esophageal cysts are common in this compartment.

Castleman's disease

Castleman's disease is a complex lymphoproliferative disease and is classified into two major subgroups: localized and multicentric Castleman's disease (MCD). Histologically, Castleman's disease is classified as hyaline-vascular (91%) and plasma cell type (9%) [28]. Castleman's disease is common in the thorax and is reported to occur in the middle (29% of thoracic cases), posterior (21%), and anterior mediastinum (17%) [29]. Hyaline-vascular Castleman's disease typically presents as a solitary mass with intense enhancement on contrast-enhanced CT (Fig. 10) and MRI. Feeding vessels (Fig. 10) and flow voids may be seen in the mass, reflecting the hypervascularity of the tumor. MCD shows multiple lymph node enlargements and interstitial lung lesions [29].

Fig. 10 Castleman's disease (hyaline-vascular type) in a 35-year-old woman. An axial contrast-enhancement CT image shows a large mass (arrow) with heterogeneous enhancement in the middle mediastinum. Feeding vessels (arrowheads) are seen in the mass, reflecting the hypervascularity of the tumor. Bilateral pleural effusion is also seen

Bronchogenic cyst and esophageal cyst

Bronchogenic cysts and esophageal (duplication) cysts result from abnormal budding of the foregut during embryologic development. Bronchogenic cysts do not usually communicate with the bronchial tree and are lined with pseudostratified columnar respiratory epithelium, and their walls usually contain cartilage, smooth muscle, and mucous gland tissue [26]. Bronchogenic cysts commonly occur in the near carina and in the paratracheal region. Esophageal cysts are lined by gastrointestinal tract mucosa, have a double layer of smooth muscle, and usually occur adjacent to or within the lower esophageal wall (Fig. 11) [26]. Imaging features of bronchogenic cysts and esophageal cysts are similar, but esophageal cyst walls, which contain a double layer of smooth muscle, may be thick (Fig. 11). Foregut cysts are usually unilocular and may have calcification. The cyst fluid is usually serous but can contain various amounts of protein and calcium and can be hemorrhagic or highly viscous. Fluid with high amounts of protein and calcium or hemorrhage may show high attenuation on CT and high signal intensity on T1-weighted images (Fig. 11b), and the cyst may mimic a solid mass [30, 31].

Posterior mediastinum (JART), paravertebral compartment (ITMIG)

The majority of solid lesions in this compartment are neurogenic tumors although rare solid and cystic lesions have also been known to occur here.

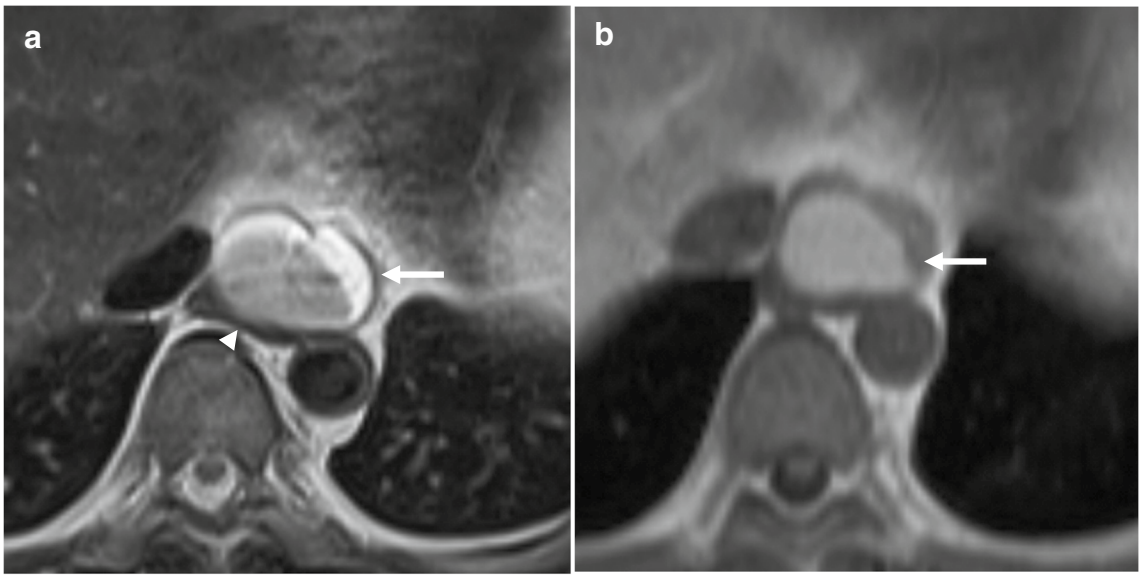

Fig. 11 Esophageal cyst in a 29-year-old man. **a** An axial T2-weighted image shows a thick-walled cyst (arrow) adjacent to the lower esophagus (arrowhead) in the middle mediastinum. The dorsal aspect of the cyst fluid shows relatively low signal intensity. **b** An axial T1-weighted image shows high signal intensity of the cyst fluid, reflecting its viscosity

Myelolipoma

Myelolipomas are benign tumors containing hematopoietic and mature adipose tissues. They are common in the adrenal glands and are very rare in the mediastinum (3% of all myelolipomas). Most mediastinal myelolipomas are located in the posterior mediastinum (92% of reported cases), with rare cases observed in the anterior mediastinum (8%) [32]. They appear as a well-circumscribed solid mass containing adipose and hematopoietic tissues.

Extramedullary hematopoiesis

Extramedullary hematopoiesis is regarded as a physiological compensatory mechanism that occurs when the bone marrow is unable to maintain sufficient red cell production to supply body demand. It tends to occur in patients with thalassemia, hereditary spherocytosis, and other hematological disorders. Extramedullary hematopoiesis is most often found in the liver and spleen but can occur in the mediastinum [33]. Intrathoracic extramedullary hematopoiesis shows well-circumscribed paravertebral masses, usually bilateral and multiple and caudal to the six thoracic vertebrae. Extramedullary hematopoiesis appears as a soft tissue mass on CT and MRI, and fatty metamorphosis in the lesion may be seen [33].

Lateral meningocele

An intrathoracic meningocele is an anomalous herniation of the leptomeninges through an intervertebral foramen or a defect in the vertebral body and is common in patients with neurofibromatosis type 1 (NF1) [26]. CT and MRI show a thin-wall paravertebral cyst which connects to the spinal dural space and contains serous cerebrospinal fluid (Fig. 12). Skeletal deformities such as dilatation of the neural foramen (Fig. 12), kyphoscoliosis, scalloping of the vertebrae, and thinning of the ribs are common [26].

Neurenteric cyst

Neurenteric cysts result from incomplete separation of the endoderm from the notochord and usually have either a fibrous connection to the spine or an intraspinal component. Neurenteric cysts are pathologically identical to esophageal duplication cysts and frequently contain both neural and enteric tissue, including gastric mucosa [20]. CT and MRI show a thin-walled paravertebral cystic mass with vertebral anomalies and intraspinal extension of the cyst [20].

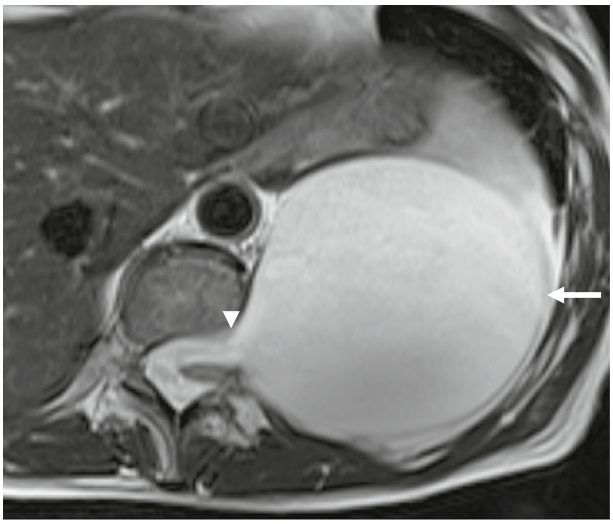

Fig. 12 Lateral meningocele in a 28-year-old woman. An axial T2-weighted image shows a thin-wall paravertebral cyst (arrow) connecting the spinal dural space and containing serous cerebrospinal fluid. Dilatation of the left neural foramen (arrowhead) is seen

Thoracic duct cyst

Thoracic duct cysts are rare benign cystic lesions thought to arise from congenital or degenerative weakening in the thoracic duct wall [34]. Thoracic duct cysts occur anywhere along the course of the thoracic duct and occasionally communicate with the duct. They can be located in the posterior or middle mediastinum, or the superior portion of the mediastinum. Thoracic duct cysts are typically a thin-walled unilocular cyst containing chylous fluid [34].

Anatomy of nerves and neurogenic tumors in the mediastinum

Neurogenic tumors are generally grouped into three categories according to tumor origin within the mediastinal nervous tissues, namely the peripheral nerves, sympathetic nerves, or paraganglia. The majority of mediastinal neurogenic tumors are peripheral nerve tumors and occur in the posterior mediastinum; however, some peripheral nerve tumors and aortopulmonary paragangliomas can occur in other mediastinal compartments. For diagnosis of mediastinal neurogenic tumors, it is important recognize the anatomy of mediastinal nerves. Figure 13 presents the anatomy of the mediastinal nerves on axial CT images, and Table 4 presents the locations of the mediastinal nerves according to the JART and ITMIG CT-based mediastinal compartment classifications.

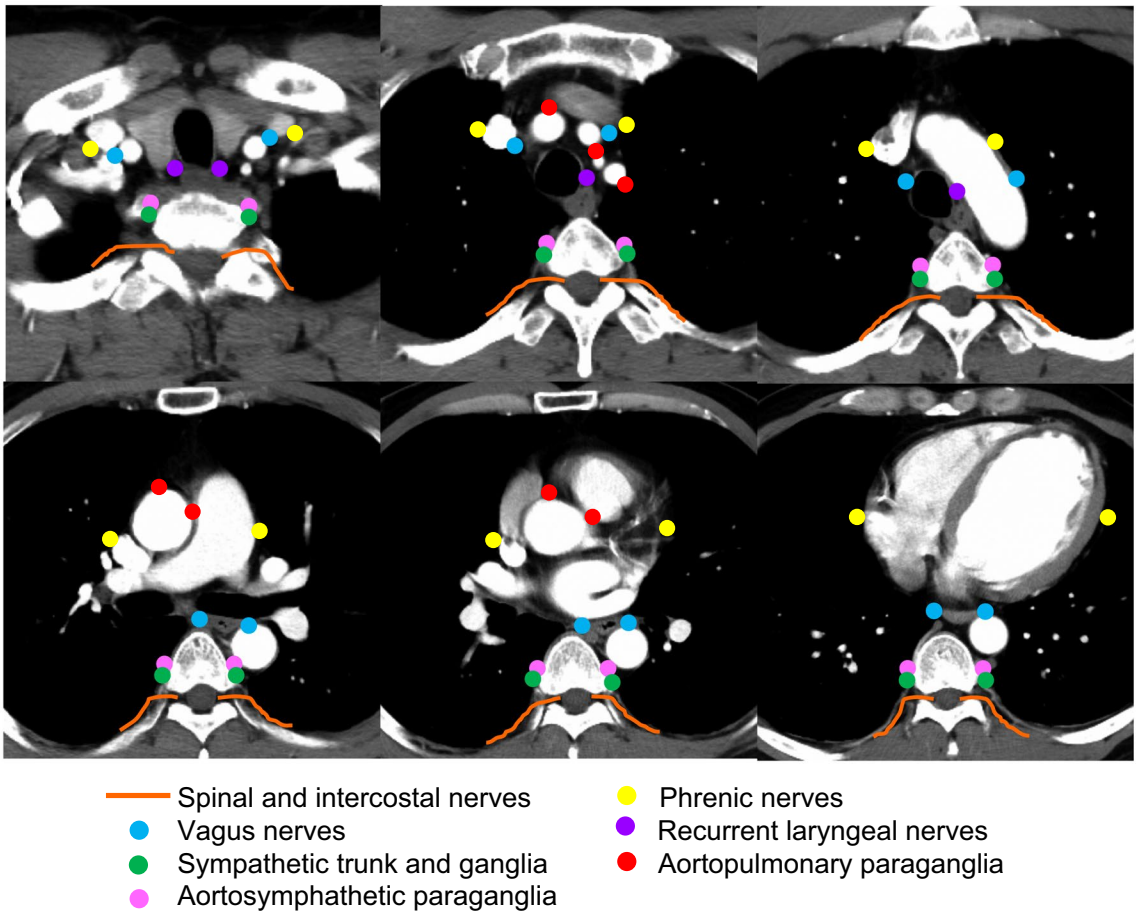

Fig. 13 Contrast-enhanced CT images represent the anatomy of the mediastinal nerves

Spinal and intercostal nerves

Twelve pairs of thoracic spinal nerves emerge from the spinal column through the intervertebral foramen. Each spinal nerve has dorsal and ventral roots. The dorsal roots connect to the intercostal nerves, and the ventral roots have fusiform spinal nerve ganglia [1]. At the back of the chest, the intercostal nerves run between the pleura and external intercostal membranes, but in the most of their course they run between the internal intercostal muscles and innermost intercostal muscles below the intercostal arteries and veins [1]. Peripheral nerve tumors arising from the spinal and intercostal nerves occur in the superior portion of the mediastinum and the posterior mediastinum (JART), and in the paravertebral compartment (ITMIG) (Fig. 14). Peripheral nerve tumors arising from the spinal nerves can locate in the paravertebral region and spinal canal through the neural foramen and show a dumbbell or hourglass shape.

Brachial plexus

The brachial plexus is a network of nerves formed by the anterior rami of the lower four cervical nerves and first thoracic nerve. This plexus extends from the spinal cord, through the cervicoaxillary canal in the neck, over the first rib, and into the axilla [1]. Peripheral nerve tumors arising from the brachial plexus protrude to the superior portion of the mediastinum (JART) and can locate in the paravertebral and visceral compartments (ITMIG) (Figs. 15, 16).

Phrenic nerves

The phrenic nerves originate mainly from the 4th cervical nerve and pass between the subclavian arteries and veins and enter the thorax [1]. The phrenic nerves cross the root of the lung anteriorly and pass over the heart between the pericardium and mediastinal pleura [1]. Peripheral nerve tumors arising from the phrenic nerves occur in the superior portion

Table 4 Locations of mediastinal nerves according to the CT-based mediastinal compartment classifications

Nerves	JART compartments	ITMIG compartments
Spinal and intercostal nerves	Superior portion Posterior	Paravertebral
Brachial plexus	Superior portion	Paravertebral (Visceral)
Phrenic nerves	Superior portion Anterior	Prevascular
Right vagus nerve	Superior portion Middle	Visceral
Left vagus nerve	Superior portion Anterior Middle	Prevascular Visceral
Recurrent laryngeal nerves	Superior portion Middle	Visceral
Sympathetic trunk and ganglia	Superior portion Posterior	Paravertebral
Aortosympathetic paraganglia	Superior portion Posterior	Paravertebral
Aortopulmonary paraganglia	Superior portion Anterior	Prevascular Visceral

JART, The Japanese Association for Research on the Thymus; ITMIG; The International Thymic Malignancy Interest Group

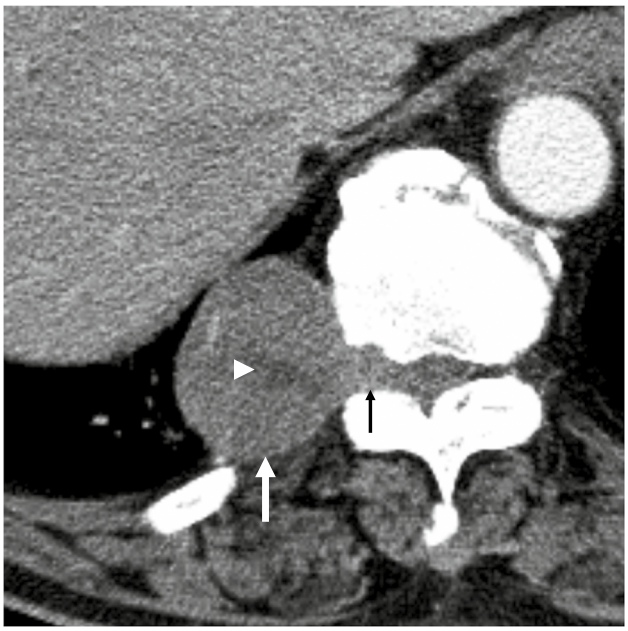

Fig. 14 Schwannoma in a 74-year-old man. An axial contrast-enhanced CT image shows a well-circumscribed mass (large arrow) in the posterior mediastinum. A central low-attenuation area (arrowhead) within the mass reflects cystic change in the tumor. The mass extends to the right neural foramen (small arrow)

of the mediastinum and the anterior mediastinum (JART), and in the prevascular compartment (ITMIG).

Vagus and recurrent laryngeal nerves

The vagus nerves originate from the medulla and extend through the jugular foramen and carotid sheath. The right vagus nerve passes between the right subclavian artery and vein, and the left vagus nerve passes between left common carotid artery and left subclavian artery, then they enter the thorax [1]. Bilateral vagus nerves descend along the esophagus in the mediastinum and contributes to cardiac, pulmonary, and esophageal plexuses. The right recurrent laryngeal nerve arises from the right vagus nerve, hooks around the right subclavian artery, and ascends between the trachea and esophagus [1]. The left vagus nerve descends on the lateral side of the aortic arch and gives rise to the left recurrent laryngeal nerve, which hooks around the aortic arch and ascends between the trachea and esophagus [1]. Peripheral nerve tumors arising from the right vagus nerve occur in the superior portion of the mediastinum and middle mediastinum (JART), and in the visceral compartment (ITMIG). Left vagus nerve tumors occur in the superior portion of the mediastinum (Fig. 17) and the anterior and middle mediastinum (JART), and in the prevascular and

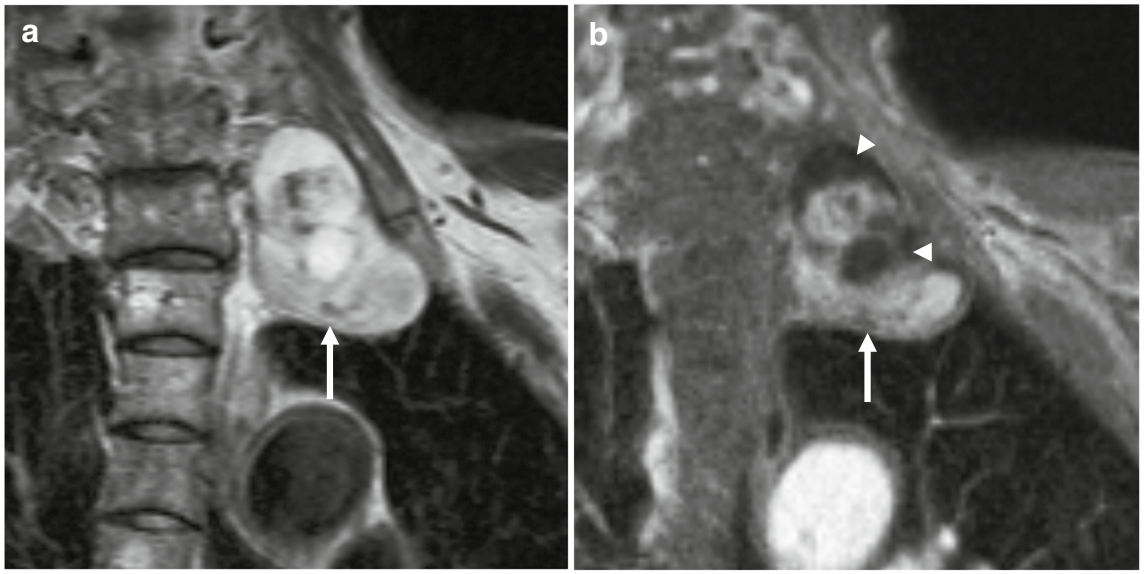

Fig. 15 Schwannoma arising from the left brachial plexus in a 59-year-old woman. **a** A coronal T2-weighted coronal image shows a well-circumscribed heterogeneous mass (arrow) in the superior portion of the mediastinum (JART). **b** A coronal contrast-enhanced T1-weighted image with fat saturation shows heterogeneous enhancement and cystic areas (arrowheads) in the mass (arrow)

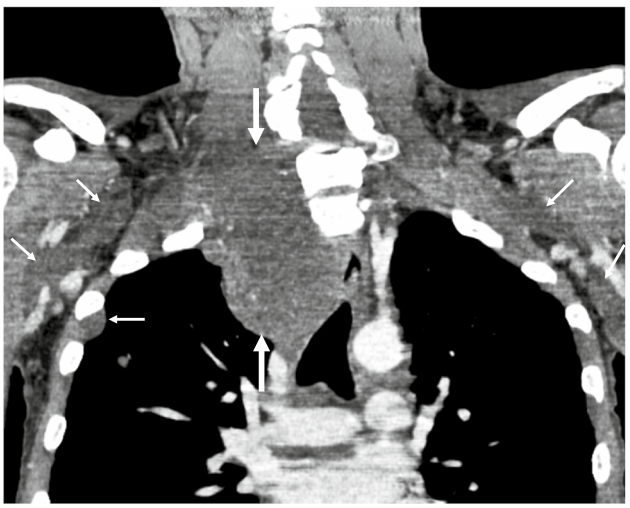

Fig. 16 Malignant peripheral nerve sheath tumor arising from the right brachial plexus in a 27-year-old man with neurofibromatosis type 1 who had pain of the right upper extremity. A coronal contrast-enhanced CT image shows an ill-defined mass (large arrows) with heterogeneous enhancement in the superior portion of the mediastinum (JART). A central low-attenuation area within the mass reflects tumor necrosis. The image shows multiple low-attenuation nodules reflecting neurofibromas (small arrows) in the chest wall and bilateral axilla

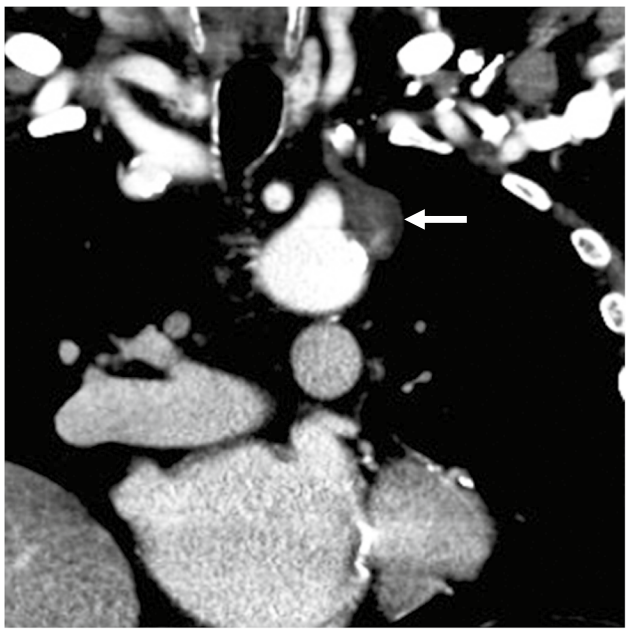

Fig. 17 Schwannoma arising from the left vagus nerve in a 70-year-old man. A coronal contrast-enhanced CT image shows a well-circumscribed nodule (arrow) with a teardrop shape in the superior portion of the mediastinum (JART)

visceral compartments (ITMIG). PNTs arising from the bilateral recurrent laryngeal nerves occur in the superior portion of the mediastinum and the middle mediastinum (JART), and in the visceral compartment (ITMIG).

Sympathetic ganglia

The sympathetic ganglia are located lateral to the vertebral body and anterior to the lateral processes. The sympathetic trunk comprises nerve fibers connecting each sympathetic

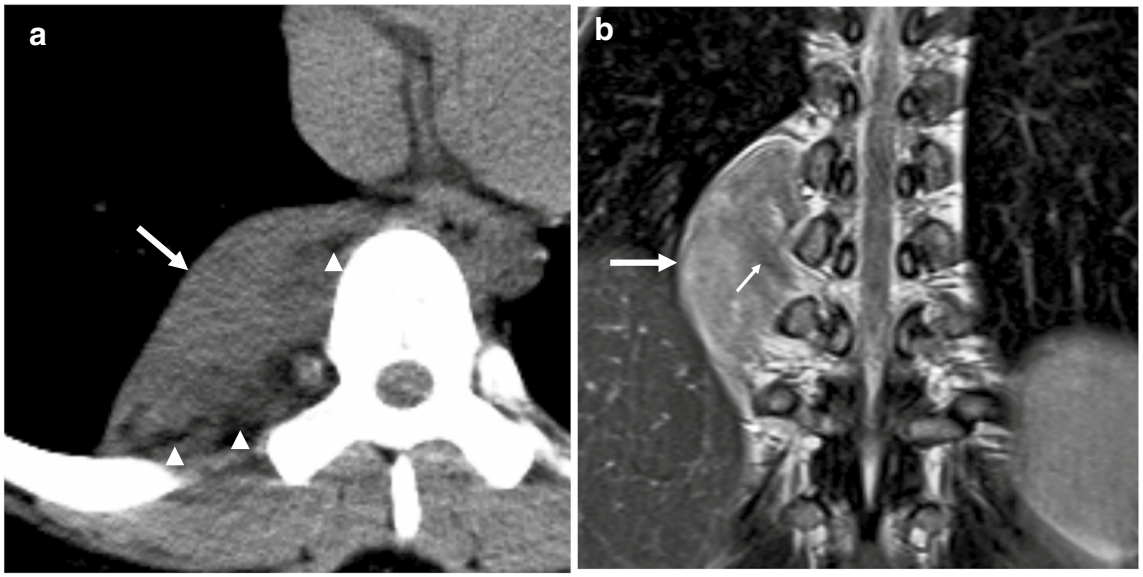

Fig. 18 Ganglioneuroma in a 15-year-old girl. **a** An axial plain CT image shows a well-circumscribed mass (arrow) in the posterior mediastinum and fat attenuation areas (arrowheads) within the mass. **b** A coronal T2-weighted image shows a vertically long mass (large arrow) with a tapered shape in the posterior mediastinum. A low-signal-intensity band (small arrow) is seen in the mass

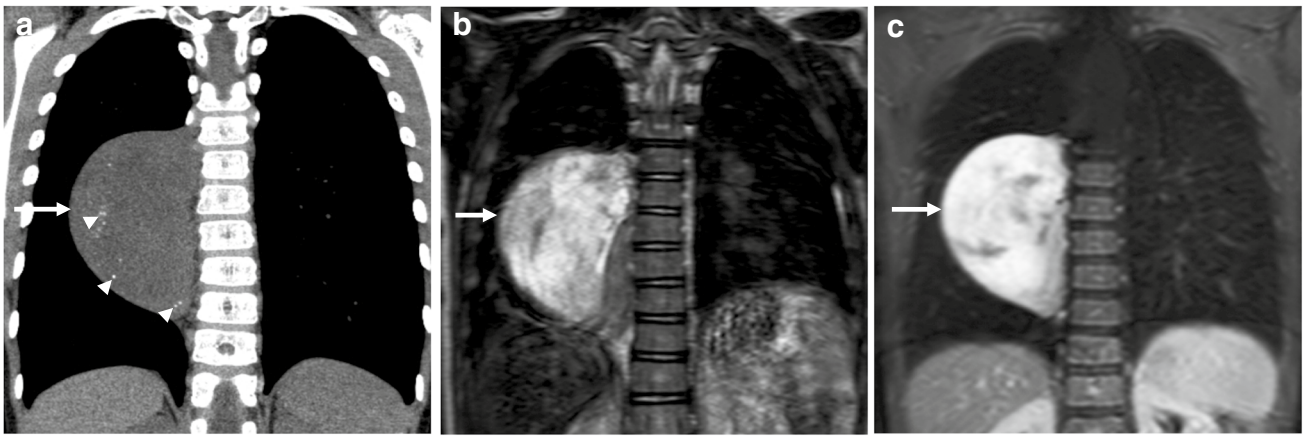

Fig. 19 Ganglioneuroblastoma in a 7-year-old girl. **a** A coronal plain CT image shows a well-circumscribed mass (arrow) in the posterior mediastinum and multiple punctate calcifications (arrowheads) within the mass. **b** A coronal T2-weighted image shows heterogeneous high signal intensity in the mass (arrow). **c** A coronal contrast-enhanced T1-weighted image with fat saturation shows heterogeneous intense enhancement in the mass (arrow)

ganglion [1]. Tumors arising from the sympathetic ganglia and trunks occur in the superior portion of the mediastinum and the posterior mediastinum (JART), and in the paravertebral compartment (ITMIG) (Figs. 18, 19).

Paraganglia

The mediastinal paraganglia are predominantly concentrated in two locations. The paraganglia found along the sympathetic chain of the paravertebral region are known as the aortosympathetic paraganglia, and those located along the great vessels are known as the aortopulmonary paraganglia, or sometimes the aortic body [35]. The aortopulmonary paraganglia are characteristically found in one of five locations within the thorax: between the ascending aorta and pulmonary trunk, either anteriorly or posteriorly, adjacent to the aortic root (the coronary paraganglia); associated with the groove between the ductus arteriosus and the pulmonary artery (the pulmonary paraganglia); between the right subclavian and right common carotid arteries; between the left subclavian and left common carotid arteries; or caudal to the left subclavian artery adjacent to the aortic arch [35].

Fig. 20 Paraganglioma in a 25-year-old woman. Axial contrast-enhanced CT image at the arterial phase shows an irregular mass (arrow) with heterogeneous enhancement between the ascending aorta and the main trunk of the pulmonary artery in the anterior mediastinum. The lesion location suggests that the tumor arises from the coronary paraganglion. Vessels (small arrow) are seen in the mass, reflecting the hypervascularity of the tumor. Invasion to the main trunk of the pulmonary artery (arrowhead) is suspected

Paraganglia in these latter four locations are also known as subclavian–supraaortic paraganglia [35]. Aortosympathetic paragangliomas occur in the superior portion of the mediastinum and the posterior mediastinum (JART), and in the paravertebral compartment (ITMIG). In contrast, aortopulmonary paragangliomas occur in the superior portion of the mediastinum and the anterior mediastinum (JART) (Fig. 20), and in the prevascular and visceral compartments (ITMIG).

Peripheral nerve tumors

Peripheral nerve tumors include schwannomas, neurofibromas, and malignant peripheral nerve sheath tumors (MPNSTs). Schwannomas are the most common mediastinal neurogenic tumor [20]. Neurofibromas account for approximately 20% of mediastinal neurogenic tumors. Multiple or plexiform neurofibromas are associated with NF1 [20]. MPNSTs are rare spindle cell sarcomas arising from a peripheral nerve or neurofibroma or showing nerve tissue differentiation. MPNSTs commonly involve major nerve trunks, such as the sciatic nerve, brachial plexus (Fig. 16), sacral plexus, or paraspinal nerves [36]. MPNSTs are associated with NF1 in 25–70% of cases, and a sudden increase in the size of a previously stable neurofibroma together with emergence of neurologic symptoms suggests malignant transformation to MPNST [36].

Paravertebral peripheral nerve tumors typically show a more markedly convex mass arising from the vertebral body compared with sympathetic nerve tumors. Cystic change (Figs. 14, 15) and hemorrhage are common in schwannomas. In schwannomas, the Antoni A area is composed of cellular spindle cells and displays relatively low signal intensity on T2-weighted images and relatively strong contrast enhancement. The Antoni B area is hypocellular and contains myxomatous loosely arranged tissue, with very high signal intensity on T2-weighted images and gradual and weak contrast enhancement. The "target sign" on T2-weigted images, comprising a peripheral high-signal-intensity area and central low-signal-intensity area, is seen in 15–54% of schwannomas, 50–70% of neurofibromas, and in 0–9% of MPNST [37–39]. Neurofibromas typically show gradual and weak contrast enhancement, which reflects myxomatous and fibrous tissues in the tumor. MPNSTs are typically heterogeneous and show peripheral enhancement due to central necrosis in the tumor on contrast-enhanced CT (Fig. 16) and MRI [36].

Sympathetic nerve tumors

Sympathetic nerve tumors include ganglioneuromas, ganglioneuroblastomas, and neuroblastomas. Ganglioneuromas are a benign tumor and are most often located in the posterior mediastinum (42% of ganglioneuromas) [40]. The median age of patients is approximately 7 years [40]. Some ganglioneuromas can arise from neuroblastoma or ganglioneuroblastoma after chemotherapy [40]. Neuroblastomas are a primitive neoplasm of neuroectodermal origin, with a median age at diagnosis of 22 months [40]. Ganglioneuroblastomas show intermediate features in cellular maturity between neuroblastoma and ganglioneuroma, and the patients are usually younger than 10 years [40]. Twenty percent of neuroblastomas and ganglioneuroblastomas occur in the posterior mediastinum [40].

Sympathetic nerve tumors show a vertically oriented mass along the anterolateral surface of several vertebrae, with a tapered appearance (Figs. 18, 19). Ganglioneuromas manifest as a well-defined mass with heterogeneous high signal intensity on T2-weighted images (Fig. 18b), reflecting myxomatous matrices in the tumors. The so-called "whorled appearance", identified by curvilinear bands of low signal intensity on T2-weighted images (Fig. 18b), reflects collagenous fibrous tissue in the tumor [41] and is seen in 50% of ganglioneuroma cases [42]. Fat can be seen in 6–29% of ganglioneuromas on CT (Fig. 18a) or MRI [42, 43]. Differential diagnosis of posterior mediastinal solid tumors with fat includes myelolipoma and extramedullary hematopoiesis.

Punctate or linear calcification is seen in 25–38% of ganglioneuroma cases on CT [42, 43]. Neuroblastomas and ganglioneuroblastomas typically show a well-or ill-defined mass with heterogeneity due to tumor necrosis [40]. Calcification (Fig. 19a) and hemorrhage in the tumor are frequent. Invasion and lymphomatous and/or hematogenous metastasis can be seen in neuroblastomas and ganglioneuroblastomas [40].

Paraganglioma

Approximately 2.5% of extraadrenal paragangliomas occur in the mediastinum [44]. Aortosympathetic paragangliomas occur in younger adults (mean age, 29 years), and half the patients present with symptoms related to the functional activity of the tumor. In contrast, aortopulmonary paragangliomas are usually asymptomatic and occur in individuals older than 40 years [45]. Paragangliomas appear as a well-or ill-defined mass and may be heterogeneous because of hemorrhage or necrosis (Fig. 20). Paragangliomas are a hypervascular tumor and may show feeding vessels peripherally and within the mass on contrast-enhanced CT (Fig. 20). Dynamic contrast-enhanced MRI shows rapid intense enhancement in the mass [46]. Adjacent high- and low-signal-intensity regions in the tumor on T2-weighted images have been described as a "salt-and-pepper" appearance [47]. The salt component, representing the high-signal-intensity regions, is due to slow flow within tumor vessels or hemorrhage while the pepper component corresponds to high flow within tumor vessels [47].

Conclusions

Mediastinal lesions comprise a variety of solid and cystic tumors. Recognition of the mediastinal anatomy, tumor location, and imaging features is important for performing differential diagnosis. There are some differences between the CT-based 4-compartment JART and 3-compartment ITMIG classification systems; each has its strengths and weaknesses. Both classification systems can improve tumor localization, streamline differential diagnosis and assist in the fine-tuning of biopsy and treatment plans.

Funding The authors declare they have no funding.

Compliance with ethical standards

Conflict of interest The authors declare that they have no conflict of interest.

Ethical standards This article does not contain any studies with human participants or animals performed by any of the authors.

References

1. Davies DV, Coupland RE. Gray's anatomy: descriptive and applied. London: Longmans, Green, & Company; 1958.
2. Felson B. Chest roentgenology. Philadelphia: WB Saunders; 1973.
3. Fraser RG, Para JA. Diagnosis of diseases of the chest. Philadelphia: WB Saunders; 1973.
4. Heitzman ER. The mediastinum, radiologic correlation with anatomy and pathology. St. Louis: CV Mosby; 1977.
5. Whitten CR, Khan S, Munneke GJ, Grubnic S. A diagnostic approach to mediastinal abnormalities. Radiographics. 2007;27:657–71.
6. Zylak CJ, Pallie W, Jackson R. Correlative anatomy and computed tomography. A module on the mediastinum. Radiographics. 1982;2:555–92.
7. Fujimoto K, Hara M, Tomiyama N, Kusumoto M, Sakai F, Fujii Y. Proposal for a new mediastinal compartment classification of transverse plane images according to the Japanese Association for Research on the Thymus (JART) general rules for the study of mediastinal tumors. Oncol Rep. 2014;31:565–72.
8. Carter BW, Tomiyama N, Bhora FY, et al. A modern definition of mediastinal compartments. J Thorac Oncol. 2014;9:S97–101.
9. Sone S, Higashihara T, Morimoto S, et al. Potential spaces of the mediastinum: CT pneumomediastinography. AJR Am J Roentgenol. 1982;138:1051–7.
10. Strollo DC, Rosado de Christenson ML, Jett JR. Primary mediastinal tumors. Part 1: tumors of the anterior mediastinum. Chest. 1997;112:511–22.
11. Clark OH. Mediastinal parathyroid tumors. Arch Surg. 1988;123:1096–100.
12. Travis WD, Brambilla E, Burke AP, Marx A, Nicholson AG. WHO classification of tumours of the lung, pleura, thymus and heart. 4th ed. Lyon: International Agency for Research on Cancer (IARC); 2015.
13. Sadohara J, Fujimoto K, Müller NL, et al. Thymic epithelial tumors: comparison of CT and MR imaging findings of low-risk thymomas, high-risk thymomas, and thymic carcinomas. Eur J Radiol. 2006;60:70–9.
14. Tomiyama N, Johkoh T, Mihara N, et al. Using the World Health Organization classification of thymic epithelial neoplasms to describe CT findings. AJR Am J Roentgenol. 2002;179:881–6.
15. Kan X, Wang P, Gong Z, Gao F, Zhang Y, Ge Y. Investigation on computed tomography features of primary thymic atypical carcinoid tumors. J Comput Assist Tomogr. 2017;41:990–4.
16. Shimamoto A, Ashizawa K, Kido Y, et al. CT and MRI findings of thymic carcinoid. Br J Radiol. 2017;90:20150341.
17. Takahashi K, Al-Janabi NJ. Computed tomography and magnetic resonance imaging of mediastinal tumors. J Magn Reson Imaging. 2010;32:1325–39.
18. Inaoka T, Takahashi K, Mineta M, et al. Thymic hyperplasia and thymus gland tumors: differentiation with chemical shift MR imaging. Radiology. 2007;243:869–76.
19. Rosado-de-Christenson ML, Pugatch RD, Moran CA, Galobardes J. Thymolipoma: analysis of 27 cases. Radiology. 1994;193:121–6.
20. Strollo DC, Rosado-de-Christenson ML, Jett JR. Primary mediastinal tumors: part II. Tumors of the middle and posterior mediastinum. Chest. 1997;112:1344–57.
21. Tateishi U, Müller NL, Johkoh T, et al. Primary mediastinal lymphoma: characteristic features of the various histological subtypes on CT. J Comput Assist Tomogr. 2004;28:782–9.
22. Kuroki S, Nasu K, Murakami K, et al. Thymic MALT lymphoma: MR imaging findings and their correlation with histopathological findings on four cases. Clin Imaging. 2004;28:274–7.

23. Moeller KH, Rosado-de-Christenson ML, Templeton PA. Mediastinal mature teratoma: imaging features. AJR Am J Roentgenol. 1997;169:985–90.
24. Sasaka K, Kurihara Y, Nakajima Y, et al. Spontaneous rupture: a complication of benign mature teratomas of the mediastinum. AJR Am J Roentgenol. 1998;170:323–8.
25. Tian L, Liu LZ, Cui CY, Zhang WD, Kuang YL. CT findings of primary non-teratomatous germ cell tumors of the mediastinum—a report of 15 cases. Eur J Radiol. 2012;81:1057–61.
26. Jeung MY, Gasser B, Gangi A, et al. Imaging of cystic masses of the mediastinum. Radiographics. 2002;22:S79–93.
27. Shaffer K, Rosado-de-Christenson ML, Patz EF Jr, Young S, Farver CF. Thoracic lymphangioma in adults: CT and MR imaging features. AJR Am J Roentgenol. 1994;162:283–9.
28. Keller AR, Hochholzer L, Castleman B. Hyaline-vascular and plasma-cell types of giant lymph node hyperplasia of the mediastinum and other locations. Cancer. 1972;29:670–83.
29. McAdams HP, Rosado-de-Christenson M, Fishback NF, Templeton PA. Castleman disease of the thorax: radiologic features with clinical and histopathologic correlation. Radiology. 1998;209:221–8.
30. Murayama S, Murakami J, Watanabe H, et al. Signal intensity characteristics of mediastinal cystic masses on T1-weighted MRI. J Comput Assist Tomogr. 1995;19:188–91.
31. Nakata H, Sato Y, Nakayama T, Yoshimatsu H, Kobayashi T. Bronchogenic cyst with high CT number: analysis of contents. J Comput Assist Tomogr. 1986;10:360.
32. Shi Q, Pan S, Bao Y, Fan H, Diao Y. Primary mediastinal myelolipoma: a case report and literature review. J Thorac Dis. 2017;9:E219–25.
33. Abe T, Yachi A, Ishii Y, et al. Thoracic extramedullary hematopoiesis associated with hereditary spherocytosis. Intern Med. 1992;31:1151–4.
34. Chen F, Bando T, Hanaoka N, et al. Mediastinal thoracic duct cyst. Chest. 1999;115:584–5.
35. Balcombe J, Torigian DA, Kim W, Miller WT Jr. Cross-sectional imaging of paragangliomas of the aortic body and other thoracic branchiomeric paraganglia. AJR Am J Roentgenol. 2007;188:1054–8.
36. Murphey MD, Smith WS, Smith SE, Kransdorf MJ, Temple HT. From the archives of the AFIP. Imaging of musculoskeletal neurogenic tumors: radiologic-pathologic correlation. Radiographics. 1999;19:1253–80.
37. Bhargava R, Parham DM, Lasater OE, Chari RS, Chen G, Fletcher BD. MR imaging differentiation of benign and malignant peripheral nerve sheath tumors: use of the target sign. Pediatr Radiol. 1997;27:124–9.
38. Jee WH, Oh SN, McCauley T, et al. Extraaxial neurofibromas versus neurilemmomas: discrimination with MRI. AJR Am J Roentgenol. 2004;183:629–33.
39. Varma DG, Moulopoulos A, Sara AS, et al. MR imaging of extracranial nerve sheath tumors. J Comput Assist Tomogr. 1992;16:448–53.
40. Lonergan GJ, Schwab CM, Suarez ES, Carlson CL. Neuroblastoma, ganglioneuroblastoma, and ganglioneuroma: radiologic-pathologic correlation. Radiographics. 2002;22:911–34.
41. Sakai F, Sone S, Kiyono K, et al. Intrathoracic neurogenic tumors: MR-pathologic correlation. AJR Am J Roentgenol. 1992;159:279–83.
42. Kato M, Hara M, Ozawa Y, Shimizu S, Shibamoto Y. Computed tomography and magnetic resonance imaging features of posterior mediastinal ganglioneuroma. J Thorac Imaging. 2012;27:100–6.
43. Guan YB, Zhang WD, Zeng QS, Chen GQ, He JX. CT and MRI findings of thoracic ganglioneuroma. Br J Radiol. 2012;85:e365–72.
44. Erickson D, Kudva YC, Ebersold MJ, et al. Benign paragangliomas: clinical presentation and treatment outcomes in 236 patients. J Clin Endocrinol Metab. 2001;86:5210–6.
45. Lee KY, Oh YW, Noh HJ, et al. Extraadrenal paragangliomas of the body: imaging features. AJR Am J Roentgenol. 2006;187:492–504.
46. Takashima Y, Kamitani T, Kawanami S, et al. Mediastinal paraganglioma. Jpn J Radiol. 2015;33:433–6.
47. Olsen WL, Dillon WP, Kelly WM, Norman D, Brant-Zawadzki M, Newton TH. MR imaging of paragangliomas. AJR Am J Roentgenol. 1987;148:201–4.